

# Journal of Materials Chemistry C

Accepted Manuscript



This article can be cited before page numbers have been issued, to do this please use: X. Gu, Y. Wang, T. Zhang, D. Liu, R. Zhang, P. Zhang, J. Wu, Z. D. Chen and S. Li, *J. Mater. Chem. C*, 2017, DOI: 10.1039/C7TC03845C.



This is an Accepted Manuscript, which has been through the Royal Society of Chemistry peer review process and has been accepted for publication.

Accepted Manuscripts are published online shortly after acceptance, before technical editing, formatting and proof reading. Using this free service, authors can make their results available to the community, in citable form, before we publish the edited article. We will replace this Accepted Manuscript with the edited and formatted Advance Article as soon as it is available.

You can find more information about Accepted Manuscripts in the [author guidelines](#).

Please note that technical editing may introduce minor changes to the text and/or graphics, which may alter content. The journal's standard [Terms & Conditions](#) and the ethical guidelines, outlined in our [author and reviewer resource centre](#), still apply. In no event shall the Royal Society of Chemistry be held responsible for any errors or omissions in this Accepted Manuscript or any consequences arising from the use of any information it contains.

# Enhanced Electronic Transport in Fe<sup>3+</sup>-doped TiO<sub>2</sub> for High Efficiency Perovskite Solar Cells

Xiangling Gu,<sup>a</sup> Yafei Wang,<sup>a</sup> Ting Zhang,<sup>a</sup> Detao Liu,<sup>a</sup> Rui Zhang,<sup>a</sup> Peng Zhang,<sup>a</sup>

Jiang Wu,<sup>c</sup> Zhi David Chen,<sup>\*ab</sup> and Shibin Li <sup>\*a</sup>

<sup>a</sup>School of Optoelectronic Information, State Key Laboratory of Electronic Thin Films and Integrated Devices, University of Electronic Science and Technology of China (UESTC), Chengdu, 610054, China

<sup>b</sup>Department of Electrical & Computer Engineering and Center for Nanoscale Science & Engineering, University of Kentucky, Lexington, Kentucky 40506, USA

<sup>c</sup>Department of Electronic and Electrical Engineering, University College London, Torrington Place, London WC1E 7JE, United Kingdom

\*Email - shibinli@uestc.edu.cn

**Abstract**

Oxygen vacancies in non-stoichiometric TiO<sub>2</sub> electron transport layer can capture injected electrons and act as recombination centers. In this study, the compact TiO<sub>2</sub> electron transport layer of perovskite solar cells (PSCs) is doped with different molar ratios of Fe<sup>3+</sup> in order to passivate such defects and improve its electron transport property. The electrical conductivity, absorption, crystal structure, and the performance of the PSCs are systematically studied. It shows that Fe<sup>3+</sup>-doping improves the conductivity of TiO<sub>2</sub> compact layer compared with the pristine TiO<sub>2</sub>, boosting the photovoltaic performance of PSCs. The reduced trap-filled limit voltage ( $V_{TFL}$ ) of the Fe<sup>3+</sup>-doped TiO<sub>2</sub> compact layer suggests that trap density in the Fe<sup>3+</sup>-TiO<sub>2</sub> film is much lower than that of a pristine TiO<sub>2</sub> film. With the optimized doping concentration (1 mol%) of Fe<sup>3+</sup>, the best power conversion efficiency of PSCs is improved from 16.02% to 18.60%.

Keywords: Fe<sup>3+</sup>-doped TiO<sub>2</sub>, electronic transport, perovskite solar cells, oxygen vacancies, conductivity

## 1. Introduction

The past several years have witnessed the fast development of a brand-new type of solar cell based on organic-inorganic halide perovskite materials.<sup>1,2</sup> The power conversion efficiency (PCE) of perovskite solar cells (PSCs) has rapidly increased from 3.8% to 22.1% since it was first reported in 2009.<sup>3-8</sup> For PSCs, the electron transport layer (ETL) plays a significant role in transporting electrons and blocking holes. In the vast majority of PSCs, TiO<sub>2</sub> is the preferred material for ETL because of its superior electronic properties.<sup>9-12</sup> For example, the conduction band of TiO<sub>2</sub> matches well with that of the perovskite active layer. Meanwhile, TiO<sub>2</sub> is low-cost, compatible with various deposition methods, chemically stable and highly conductive.<sup>12-17</sup> However, there exist oxygen vacancies, Ti interstitial sites, and trap states in TiO<sub>2</sub> ETL, which can capture injected electrons and act as recombination centers. As a result, these defects and trap states dramatically degrade the efficiency and stability of devices.<sup>18-21</sup> Therefore, fabrication of a TiO<sub>2</sub> ETL with reduced oxygen vacancies and defects is critical to improve the charge extraction and collection of PSCs.

Previous works have demonstrated that it can effectively enhance electron transport in the TiO<sub>2</sub> by doping suitable metal ions. In 2014, Snaith's group doped Al into a TiO<sub>2</sub> compact layer and found that the conductivity of TiO<sub>2</sub> compact layer was increased by several orders of magnitude due to reduced oxygen vacancies in the TiO<sub>2</sub> ETL.<sup>20</sup> Zhou *et al.* reported that yttrium-doped TiO<sub>2</sub> compact layer improved the conductivity and carrier extraction ability of the ETL, and enhanced the cell's PCE to

19.3%.<sup>22</sup> In addition, Zn-doped, Nb-doped, Mg-doped and Li-doped TiO<sub>2</sub> ETLs have also been reported.<sup>23-28</sup> However, very limited study has been reported on Fe-doped TiO<sub>2</sub> ETL for perovskite solar cells. Previous studies of Fe-doped TiO<sub>2</sub> were devoted to improving photocatalytic property, visible light activity or tuning the band-gap structure of TiO<sub>2</sub> rather than enhancing its electrical properties for application in PSCs.<sup>29-31</sup> For example, Yalcin *et al.* found that visible light activity and photocatalytic property of TiO<sub>2</sub> particles were improved by Fe<sup>3+</sup>-doping and the same result was reported by Zhu *et al.*<sup>29,32</sup> Fe<sup>3+</sup> has the same valence as Al<sup>3+</sup> and Y<sup>3+</sup> and similar radius to Ti<sup>4+</sup> (Fe<sup>3+</sup>=0.064nm, Ti<sup>4+</sup>=0.068nm).<sup>33</sup> Therefore, Fe<sup>3+</sup> cations can penetrate into the TiO<sub>2</sub> lattice and substitute Ti cations.<sup>29</sup> One would expect that Fe<sup>3+</sup>-doped TiO<sub>2</sub> ETLs could lead to further improved photovoltaic performance of PSCs compared with other doped ETLs.

In this work, we doped a TiO<sub>2</sub> compact layer with Fe<sup>3+</sup> ions (Fe<sup>3+</sup>-TiO<sub>2</sub>) and used it as ETL for perovskite solar cells. The Fe<sup>3+</sup>-doped TiO<sub>2</sub> precursor solution can be obtained easily through mixing Fe(NO<sub>3</sub>)<sub>3</sub> solution with TiO<sub>2</sub> solution in proper proportion, including 0.5 mol%, 1 mol%, 2 mol%, and 5 mol%. As a result of Fe<sup>3+</sup> doping, we demonstrate that the conductivity increases significantly by an order of magnitude and the trap-filled limit voltage ( $V_{TFL}$ ) of the Fe<sup>3+</sup>-doped TiO<sub>2</sub> compact layer obviously decreases compared with the pure TiO<sub>2</sub> compact layer.<sup>34</sup> Consequently, we obtain a high efficiency of 18.01% for MAPbI<sub>3</sub>-based solar cells and 18.6% for Cs<sub>0.05</sub>(MA<sub>0.17</sub>FA<sub>0.83</sub>)<sub>0.95</sub>Pb(I<sub>0.83</sub>Br<sub>0.17</sub>)<sub>3</sub>-based cells. The results reported in this work demonstrate the performance of PSCs can be enhanced by doping TiO<sub>2</sub> compact layer

with  $\text{Fe}^{3+}$  ions.

## 2. Results and discussion

As shown in Fig. 1a, the mesoporous-structure perovskite solar cells, consisting of FTO/  $\text{Fe}^{3+}$ - $\text{TiO}_2$  (or  $\text{TiO}_2$ )/ meso- $\text{TiO}_2$ /  $\text{MAPbI}_3$ / Spiro-OMeTAD/ Au, are fabricated. Fig. 1b and c are the scanning electron microscopy (SEM) images of the pristine  $\text{TiO}_2$  and 1 mol%  $\text{Fe}^{3+}$ - $\text{TiO}_2$  layers. The results show that both the  $\text{Fe}^{3+}$ - $\text{TiO}_2$  and pure  $\text{TiO}_2$  compact layers are uniform and homogeneous. The SEM cross-sectional image of a PSC in Fig. 1d shows that perovskite thin films with large crystalline grains are prepared. Fig. 1e exhibits that the color of the  $\text{Fe}^{3+}$ - $\text{TiO}_2$  solution gradually changes to red with the increase of doping concentration. In order to investigate the distribution of Fe elements, we measured energy dispersive spectrometer (EDS) spectra at five separated positions for the 5 mol%  $\text{Fe}^{3+}$ - $\text{TiO}_2$  film ( $\approx 700$  nm). As displayed in Fig. S1, S2 and Table 1, the atomic ratios of Fe/Ti at five positions show a small difference, and the obtained average atomic ratio in EDS analysis is 6.4%. The EDS result confirms that Fe element is homogeneously distributed within  $\text{TiO}_2$  film.

X-ray diffraction (XRD) measurement is conducted to elucidate the lattice structure. As shown in Fig. 2a, all the  $\text{TiO}_2$  compact layers doped with different doping concentrations are anatase phase. This is because the ionic radius of  $\text{Fe}^{3+}$  is very similar to  $\text{Ti}^{4+}$ , and the  $\text{Fe}^{3+}$  dopants cannot change the lattice parameter of  $\text{TiO}_2$ . In Fig. 2b, the absorption of  $\text{Fe}^{3+}$ - $\text{TiO}_2$  compact films shows enhanced visible light activity or red shift. The absorbance increases with the increase of  $\text{Fe}^{3+}$  doping

concentration. This has been attributed to the formation of a Fe-dopant energy level within the band gap of TiO<sub>2</sub>.<sup>29,31,32,35</sup> XRD patterns of MAPbI<sub>3</sub> thin films on doped and undoped TiO<sub>2</sub> compact layers shown in Fig. 2c reveal an identical crystalline structure as reported in the previous literature.<sup>36</sup> The absorption shown in Fig. 2d imply that Fe<sup>3+</sup>-doping of TiO<sub>2</sub> compact layer indicates negligible effects on the absorption of MAPbI<sub>3</sub> thin films in the range of visible light.

The current density versus voltage (J-V) curves shown in Fig. 3a reveal that the PSCs doped with 1 mol% Fe<sup>3+</sup> yield the best performance. As shown in Fig. 3b, it is known that oxygen vacancies or Ti interstitials are the predominant non-stoichiometry defects in TiO<sub>2</sub> lattice, resulting in the conversion of Ti<sup>4+</sup> to Ti<sup>3+</sup>.<sup>37-40</sup> Therefore, Ti<sup>3+</sup> defects can induce a shallow energy level below the conduction band and act as electron trap sites, which can capture electrons and reduce electron transport efficiency and conductivity of TiO<sub>2</sub>. Based on above analysis and previous literatures, as shown in Fig. 3c, two Fe<sup>3+</sup> can substitute two Ti<sup>3+</sup> adjacent to an oxygen defect. Consequently, this substitution effectively passivates or removes oxygen vacancy defects or traps in TiO<sub>2</sub> compact layer. The Fe<sup>3+</sup>-doping mechanism is consistent with that of the Al-doped TiO<sub>2</sub>. This conclusion is supported by the increased conductivity and decreased trap-filled limit voltage ( $V_{TFL}$ ) of TiO<sub>2</sub> compact layer thin film in the following study.

To explore the role of Fe<sup>3+</sup>-doping, X-ray photoelectron spectroscopy (XPS) measurement was carried out. Fig. 3d shows the XPS spectra of the Fe<sup>3+</sup>-doped and undoped TiO<sub>2</sub> samples. The binding energies in the range 710.4-712.3 eV and

724.0-724.5 eV should be assigned to  $2p_{3/2}$  and  $2p_{1/2}$  of  $\text{Fe}^{3+}$  cations.<sup>35,41</sup> The signal of Fe  $2p_{3/2}$  (1 mol%  $\text{Fe}^{3+}$ - $\text{TiO}_2$ ) is weak due to the low doping level, but still obvious compared with the pristine  $\text{TiO}_2$ . The result indicates that Fe elements doped into the  $\text{TiO}_2$  lattice are in a trivalent valence state. The atomic ratios of Fe/Ti for pristine and  $\text{Fe}^{3+}$ -doped  $\text{TiO}_2$  are shown in Table 2 and the survey XPS spectra is presented in Fig. S3. In Fig. 3e, the binding energy of O 1s peak centered at 529.13 eV and 529.19 eV can be ascribed to  $\text{TiO}_2$ . The smaller peak at 531.02 eV and 531.21 eV may be assigned to the surface hydroxyl groups or chemisorbed water molecules.<sup>32</sup> The slightly higher O 1s binding energy for the  $\text{Fe}^{3+}$ -doped sample further suggests the linkage of Fe-O-Ti bond in  $\text{Fe}^{3+}$ - $\text{TiO}_2$ . Ti  $2p_{3/2}$  and Ti  $2p_{1/2}$  peaks for all samples in Fig. 3f are located at binding energies of 457.96 eV and 463.63 eV, respectively. Perhaps, due to the low concentration of  $\text{Fe}^{3+}$ , the shift of Ti 2p peaks is below the detection limit.

It is demonstrated that the transport of photogenerated electrons in films is limited by space-charge effects.<sup>34</sup> The density of free carriers is reduced when the trap centers capture the photogenerated free carriers, leading to a smaller current with a small slope at low bias voltage. However, as the voltage is continuously increased, all the traps are filled. The current quickly increases nonlinearly with a higher slope if the bias voltage exceeds the kink point. The kink point is the trap-filled limit voltage ( $V_{\text{TFL}}$ ). So we can estimate the values of  $V_{\text{TFL}}$  by calculating the intersection of the two slopes. Furthermore,  $V_{\text{TFL}}$  can be determined by the trap-state density ( $N_t$ ).

$$V_{\text{TFL}} = \frac{eN_t d^2}{2\epsilon\epsilon_0} \quad (1)$$

Where  $e$  is the elementary charge of the electron,  $d$  and  $\varepsilon$  are the thickness and relative dielectric constant of the active layer,  $\varepsilon_0$  is the vacuum permittivity.<sup>42</sup> According to equation (1), we can see that  $V_{\text{TFL}}$  increases with the increase of trap density.

To confirm whether doping  $\text{Fe}^{3+}$  can effectively reduce the trap density in the  $\text{TiO}_2$  compact layer, we measured the log-log plot of I-V curves for  $\text{Fe}^{3+}$ -doped and undoped devices with a structure shown in the inset of Fig. 4a. The nonlinear curve in Fig. 4a indicates the existence of space charges, e.g. Ti interstitials, oxygen vacancies, etc. For the best  $\text{Fe}^{3+}$ -doping condition, the I-V curve is more linear. The  $V_{\text{TFL}}$  of 1 mol%  $\text{Fe}^{3+}$ - $\text{TiO}_2$  is estimated to be 0.45 V, which is pretty lower than that of pure  $\text{TiO}_2$  (0.64 V) and Fig. 4a shows a significant difference in current between doped and pristine samples. The result demonstrates that the trap-state density in the  $\text{Fe}^{3+}$ - $\text{TiO}_2$  film is much lower than that in a pristine  $\text{TiO}_2$  film. The reason is possibly because  $\text{Fe}^{3+}$ -doping suppresses space charges and increases the carrier density and conductivity of  $\text{TiO}_2$ . These can be verified from the results of the Hall Effect measurement. The conductivity versus dopant concentration curves and results of Hall Effect are shown in the inset of Fig. 4a and Table S1. Table S1 shows that the conductivity of  $\text{Fe}^{3+}$ -doped  $\text{TiO}_2$  is increased by an order of magnitude compared with pristine  $\text{TiO}_2$ , which is possibly caused by the increased carrier density and reduced trap states in ETL.

Fig. 4b is the hysteresis curve for the cells. Under the best doping concentration of  $\text{Fe}^{3+}$ , a high PCE of 18.01% from reverse scan and 17.22% from forward scan for

CH<sub>3</sub>NH<sub>3</sub>PbI<sub>3</sub>-based cells is obtained. We observed a slight reduction in hysteresis compared with the undoped devices. This may be attributed to Fe<sup>3+</sup> ions passivating the electronic defects or trap states caused by non-stoichiometric oxygen-induced defects within the TiO<sub>2</sub> lattice. The passivation enhanced the extraction of free electrons and suppressed the cell's hysteresis.<sup>19,20</sup> Fig. 4c shows a steady-state current density of 20.15 mA/cm<sup>2</sup> and efficiency of 17.12% after 150 s operation at a bias voltage of 0.83 V from reverse scan direction for the Fe<sup>3+</sup>-TiO<sub>2</sub>/ MAPbI<sub>3</sub>-based cell, whereas the TiO<sub>2</sub>-based control cell displays a steady-state current density of 16.24 mA/cm<sup>2</sup> and efficiency of 14.13% at a bias voltage of 0.77 V. Fig. 4d shows that the external quantum efficiency (EQE) of the Fe<sup>3+</sup>-doped device is much higher than the undoped one. The highest value for Fe<sup>3+</sup>-doped device is almost 91%, which is mainly due to enhanced electron extraction via using Fe<sup>3+</sup>-TiO<sub>2</sub>. The integrated J<sub>sc</sub> for Fe<sup>3+</sup>-doped and undoped device in Fig. 4d is 22.06 mA/cm<sup>2</sup> and 20.19 mA/cm<sup>2</sup>, respectively. According to Table 3, the PSCs with 1 mol% Fe<sup>3+</sup>-TiO<sub>2</sub> compact layer exhibit the best performance. The V<sub>oc</sub>, J<sub>sc</sub> and FF increase from 1.02 V to 1.06 V, from 22.03 mA/cm<sup>2</sup> to 23.22 mA/cm<sup>2</sup>, and from 63.25% to 66.68% (mean values with reverse scan). As a result, the average PCE is raised from 14.59% to 17.01%.

Electrochemical impedance spectroscopy (EIS) is utilized to investigate the charge-transport process and carrier recombination of the TiO<sub>2</sub>-based perovskite cells. The inset in Fig. 4e is an equivalent circuit of the cells and our test frequency is from 1Hz to 1MHz under 1 sun illumination. The parameters of carrier transport and recombination in PSCs are fitted by analyzing Nyquist curves. Normally, there are

two arcs on the Nyquist curve, where the first arc at high frequency is related to the transport and extraction in the cathode and the second arc is related to the recombination process between different layers.<sup>43-45</sup> Nyquist plot in Fig. 4e and parameters in Table S2 show that recombination resistance of Fe<sup>3+</sup>-TiO<sub>2</sub>-based cells at interfaces between different films is significantly larger than TiO<sub>2</sub>-based cells. Since a larger recombination resistance indicates a lower recombination loss, this result illustrates that the recombination process is effectively suppressed for Fe<sup>3+</sup>-TiO<sub>2</sub>-based cells. It further manifests that the Fe<sup>3+</sup>-TiO<sub>2</sub> has fewer trapping centers and improved interface properties (more information about Nyquist plot can be obtained from Electronic Supplementary Information (ESI) ).

Furthermore, to determine the junction property of the cell, a model based on the single heterojunction solar cell is adopted.<sup>46</sup> In a heterojunction solar cell, the value of the ideality factor (N) represents the quality of a junction and the carrier recombination mechanisms. The smaller value of N, the less recombination caused by defect in the cell. Calculation method of N can be found in ESI and Fig. S4 is the box plot of N at different doping concentrations. In our experiment, we calculated N for doped and undoped samples under light conditions shown in Fig. 4f and Table 3 , and the mean values of 1 mol% Fe<sup>3+</sup>-TiO<sub>2</sub> and pure TiO<sub>2</sub> perovskite cells are 2.95 and 3.99, respectively. We can see that the former is much smaller than the latter, which probably means that the carrier recombination in Fe<sup>3+</sup>-TiO<sub>2</sub> cells is reduced due to the reduction of trap states in the doped TiO<sub>2</sub> compact layer.

Fig. 5a-d are the statistics of Voc, FF, Jsc, and PCE of 100 devices based on

different doping conditions. The statistical distributions of  $V_{oc}$ ,  $J_{sc}$ , FF and PCE for the  $TiO_2$  and  $Fe^{3+}$ - $TiO_2$  based cells in Fig. 5 show that 1mol%  $Fe^{3+}$ -doped cells exhibit higher photovoltaic parameters compared with the others. Thus, photovoltaic performance of the cells can be effectively improved by doping  $Fe^{3+}$  in the ETL. The stability of MAPbI<sub>3</sub>-based cells tested for three weeks in the dark is provided, as shown in Fig. S5 and S6. The devices were exposed directly to the air without encapsulation (25%-35% relative humidity (RH), 25°C). It has been demonstrated that the degradation of PSCs is mainly ascribed to the decomposition of perovskite in air.<sup>47</sup> As shown in Fig. S5, the perovskite solar cells based on  $Fe^{3+}$ -doped and pristine  $TiO_2$  exhibited similar performance deterioration.

We also fabricated Cs/FA/MA-based PSCs with  $Fe^{3+}$ -doped compact layer as reported by Saliba.<sup>48</sup> In Fig. S7a, the device yields a high PCE of 18.60% from reverse scan and 17.88% from forward scan under best doping concentration, whereas the  $TiO_2$ -based control devices exhibited a PCE of 16.02% and 14.86% respectively. In addition, Fig. S7b shows a steady-state current density of 20.75 mA/cm<sup>2</sup> and efficiency of 17.6% for  $Fe^{3+}$ -doped Cs/FA/MA-based cell after 150 s operation from reverse scan direction at the bias voltage of 0.84 V. The results demonstrate that the high performance  $Fe^{3+}$ - $TiO_2$ -based PSCs is repeatable. Detailed parameters of the devices are presented in the inset table of Fig. S7a.

### 3. Conclusions

In summary, we fabricated MAPbI<sub>3</sub>-based and Cs/FA/MA-based perovskite solar cells by doping compact  $TiO_2$  layer with different  $Fe^{3+}$  concentrations. Due to the

reduction of electron trap density, the Fe<sup>3+</sup>-doped TiO<sub>2</sub> compact layer shows enhanced conductivity and reduced V<sub>TFL</sub>. Therefore, Fe<sup>3+</sup>-doped compact TiO<sub>2</sub> films extract photogenerated electrons more efficiently. As a result, cells with doped ETLs are successfully improved compared with cells with pristine TiO<sub>2</sub>. Finally, the PCE is improved from 14.59% to 18.01% for MAPbI<sub>3</sub>-based cell, while the PCE of Cs/FA/MA-based cell is increased from 16.02% to 18.6%. So Fe<sup>3+</sup> doped TiO<sub>2</sub> compact layer provides a feasible way to fabricate high performance PSCs.

### Notes

The authors declare no competing financial interest.

### Acknowledgements

This work was supported by National Natural Science Foundation of China under Grant Nos. 61421002, 61574029, 61471085, and 61371046. This work was also partially supported by University of Kentucky.

### REFERENCES

- 1 M. A. Green, A. Ho-Baillie and H. J. Snaith, *Nat. Photonics*, 2014, **8**, 506-514.
- 2 D. Zheng, G. Yang, Y. Zheng, P. Fan, R. Ji, J. Huang and J. Yu, *Electrochim. Acta*, 2017, **247**, 548-557.
- 3 A. Kojima, K. Teshima, Y. Shirai and T. Miyasaka, *J. Am. Chem. Soc.*, 2009, **131**, 6050-6051.
- 4 Y. Wang, S. Li, P. Zhang, D. Liu, X. Gu, H. Sarvari and Z. D. Chen, *Nanoscale*, 2016, **8**, 19654-19661.
- 5 Y. Zhao and K. Zhu, *J. Am. Chem. Soc.*, 2014, **136**, 12241-12244.
- 6 D. Zheng, W. Huang, P. Fan, Y. Zheng, J. Huang and J. Yu, *ACS Appl. Mater. Interfaces*, 2017, **9**, 4898-4907.

- 7 W. S. Yang, B. W. Park, E. H. Jung, N. J. Jeon, Y. C. Kim, D. U. Lee and S. I. Seok, *Science*, 2017, **356**, 1376-1379.
- 8 Y. Zhao, and K. Zhu, *Chem. Soc. Rev.*, 2016, **45**, 655-689.
- 9 W. S. Yang, J. H. Noh, N. J. Jeon, Y. C. Kim, S. Ryu, J. Seo and S. I. Seok, *Science*, 2015, **348**, 1234-1237.
- 10 D. Bi, W. Tress, M. I. Dar, P. Gao, J. Luo, C. Renevier and J. D. Decoppet, *Sci. Adv.*, 2016, **2**, e1501170.
- 11 N. Ahn, D. Y. Son, I. H. Jang, S. M. Kang, M. Choi and N. G. Park, *J. Am. Chem. Soc.*, 2015, **137**, 8696-8699.
- 12 S. Li, P. Zhang, H. Chen, Y. Wang, D. Liu, J. Wu and Z. D. Chen, *J. Power Sources*, 2017, **342**, 990-997.
- 13 M. M. Lee, J. Teuscher, T. Miyasaka, T. N. Murakami and H. J. Snaith, *Science*, 2012, **338**, 643-647.
- 14 X. Li, D. Bi, C. Yi, J. D. Decoppet, J. Luo, S. M. Zakeeruddin and M. Grätzel, *Science*, 2016, **353**, 58-62.
- 15 J. Burschka, N. Pellet, S. J. Moon, R. Humphry-Baker, P. Gao, M. K. Nazeeruddin and M. Grätzel, *Nature*, 2013, **499**, 316-319.
- 16 T. Zhu and S. P. Gao, *J. Phys. Chem. C*, 2014, **118**, 11385-11396.
- 17 H. Yu, S. Zhang, H. Zhao, G. Will and P. Liu, *Electrochim. Acta*, 2009, **54**, 1319-1324.
- 18 H. S. Kim, C. R. Lee, J. H. Im, K. B. Lee, T. Moehl, A. Marchioro, S. J. Moon, R. Humphry-Baker, J. H. Yum, J. E. Moser, M. Grätzel and N. G. Park, *Sci. Rep.*, 2012, **2**, 591.
- 19 F. Giordano, A. Abate, J. P. Correa Baena, M. Saliba, T. Matsui, S. H. Im, S. M. Zakeeruddin, M. K. Nazeeruddin, A. Hagfeldt and M. Graetzel, *Nat. Commun.*, 2016, **7**, 10379.
- 20 S. K. Pathak, A. Abate, P. Ruckdeschel, B. Roose, K. C. Gödel, Y. Vaynzof and A. Sepe, *Adv. Funct. Mater.*, 2014, **24**, 6046-6055.
- 21 C. O'Rourke and D. R. Bowler, *J. Phys. Chem. C*, 2014, **118**, 7261-7271.
- 22 H. Zhou, Q. Chen, G. Li, S. Luo, T. B Song, H. S. Duan, Z. Hong, J. You, Y. Liu

- and Y. Yang, *Science*, 2014, **345**, 542-546.
- 23 D. Liu, S. Li, P. Zhang, Y. Wang, R. Zhang, H. Sarvari and Z. D. Chen, *Nano Energy*, 2017, **31**, 462-468.
- 24 M. Lv, W. Lv, X. Fang, P. Sun, B. Lin, S. Zhang, X. Xu, J. Ding and N. Yuan, *RSC Adv.*, 2016, **6**, 35044-35050.
- 25 M. Yang, R. Guo, K. Kadel, Y. Liu, K. O'Shea, R. Bone, X. Wang, J. He and W. Li, *J. Mater. Chem. A*, 2014, **2**, 19616-19622.
- 26 J. Wang, M. Qin, H. Tao, W. Ke, Z. Chen, J. Wan, P. Qin, L. Xiong, H. Lei, H. Yu and G. Fang, *Appl. Phys. Lett.*, 2015, **106**, 121104.
- 27 X. Yin, Y. Guo, Z. Xue, P. Xu, M. He and B. Liu, *Nano Res.* 2015, **8**, 1997-2003.
- 28 X. Yin, Z. Xu, Y. Guo, P. Xu and M. He, *ACS Appl. Mater. Interfaces*, 2016, **8**, 29580-29587.
- 29 Y. Yalçın, M. Kılıç and Z. Çınar, *Appl. Catal., B*, 2010, **99**, 469-477.
- 30 W. Y. Teoh, R. Amal, L. Mädler and S. E. Pratsinis, *Catal. Today*, 2007, **120**, 203-213.
- 31 S. George, S. Pokhrel, Z. Ji, B. L. Henderson, T. Xia, L. Li and L. Mädler, *J. Am. Chem. Soc.*, 2011, **133**, 11270-11278.
- 32 J. Zhu, F. Chen, J. Zhang, H. Chen and M. Anpo, *J. Photochem. Photobiol., A*, 2006, **180**, 196-204.
- 33 T. A. Egerton, E. Harris, E. J. Lawson, B. Mile and C. C. Rowlands, *Phys. Chem. Chem. Phys.*, 2001, **3**, 497-504.
- 34 R. H. Bube, *J. Appl. Phys.*, 1962, **33**, 1733-1737.
- 35 V. N. Nguyen, N. K. T. Nguyen and P. H. Nguyen, *Adv. Nat. Sci.: Nanosci. Nanotechnol.*, 2011, **2**, 035014.
- 36 Q. Dong, Y. Yuan, Y. Shao, Y. Fang, Q. Wang and J. Huang, *Energy Environ. Sci.*, 2015, **8**, 2464-2470.
- 37 A. K. Ghosh, F. G. Wakim, R. R. Addiss Jr, *Phys. Rev.*, 1969, **184**, 979.
- 38 M. A. Henderson, *Surf. Sci.*, 1999, **419**, 174-187.
- 39 M. Nolan, S. D. Elliott, J. S. Mulley, R. A. Bennett, M. Basham and P. Mulheran,

- Phys. Rev. B*, 2008, **77**, 235424.
- 40 S. Wendt, P. T. Sprunger, E. Lira, G. K. Madsen, Z. Li, J. Ø. Hansen and F. Besenbacher, *Science*, 2008, **320**, 1755-1759.
- 41 C. D. Wagner, W. M. Riggs, L. E. Davis, J. F. Moulder and G. E. Muilenberg, Handbook of X-Ray Photoelectron Spectroscopy. *Perkin-Elmer Corp., Physical Electronics Division, USA*, 1979, chapter **2**, page 42 (O), page 68 (Ti), page 76 (Fe).
- 42 J. H. Heo, M. S. You, M. H. Chang, W. Yin, T. K. Ahn, S. J. Lee and S. H. Im, *Nano Energy*, 2015, **15**, 530-539.
- 43 G. Veerappan, D. W. Jung, J. Kwon, J. M. Choi, N. Heo, G. R. Yi and J. H. Park, *Langmuir*, 2014, **30**, 3010-3018.
- 44 V. Gonzalez-Pedro, E. J. Juarez-Perez, W. S. Arsyad, E. M. Barea, F. Fabregat-Santiago, I. Mora-Sero and J. Bisquert, *Nano Lett.*, 2014, **14**, 888-893.
- 45 A. Dualeh, T. Moehl, N. Tétreault, J. Teuscher, P. Gao, M. K. Nazeeruddin, M. Grätzel, *Acs Nano*, 2013, **8**, 362-373.
- 46 J. Shi, J. Dong, S. Lv, Y. Xu, L. Zhu, J. Xiao and Q. Meng, *Appl. Phys. Lett.*, 2014, **104**, 063901.
- 47 G. Niu, W. Li, F. Meng, L. Wang, H. Dong and Y. Qiu, *J. Mater. Chem. A*, 2014, **2**, 705-710.
- 48 M. Saliba, T. Matsui, J. Y. Seo, K. Domanski, J. P. Correa-Baena, M. K. Nazeeruddin and M. Grätzel, *Energy Environ. Sci.*, 2016, **9**, 1989-1997.

## Figures and tables:

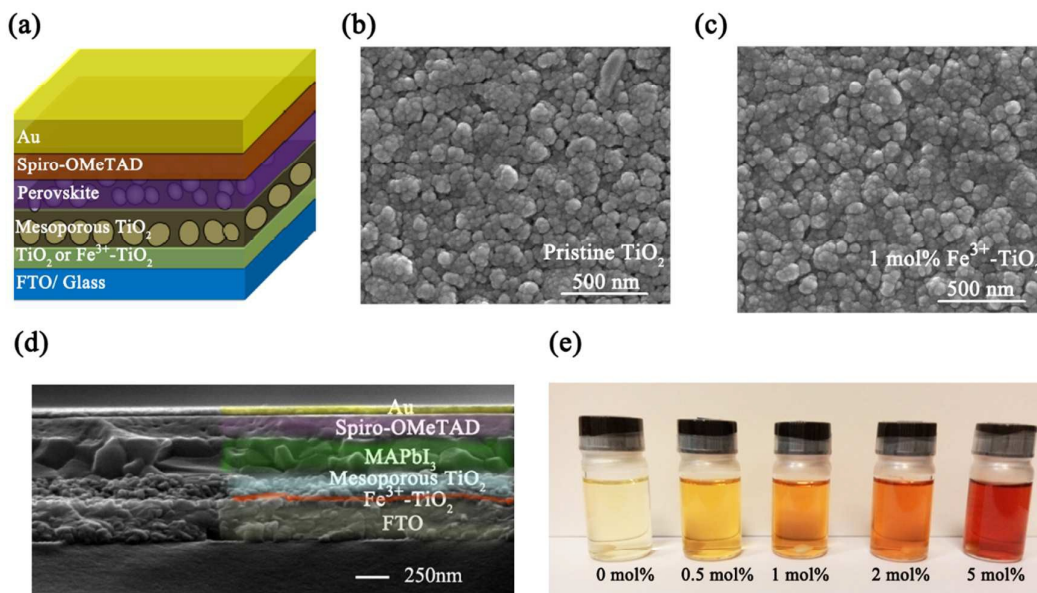


**Fig. 1** (a) Schematic diagram of mesoporous MAPbI<sub>3</sub>-based solar cell. (b) SEM image of FTO/ TiO<sub>2</sub>. (c) SEM image of FTO/ 1 mol% Fe<sup>3+</sup>-TiO<sub>2</sub>. (d) Cross-sectional SEM image of the cell with a structure: FTO/ Fe<sup>3+</sup>-TiO<sub>2</sub>/ meso-TiO<sub>2</sub>/ MAPbI<sub>3</sub>/ Spiro-OMeTAD/ Au. (e) Solutions of pristine TiO<sub>2</sub> and Fe<sup>3+</sup>-TiO<sub>2</sub>.

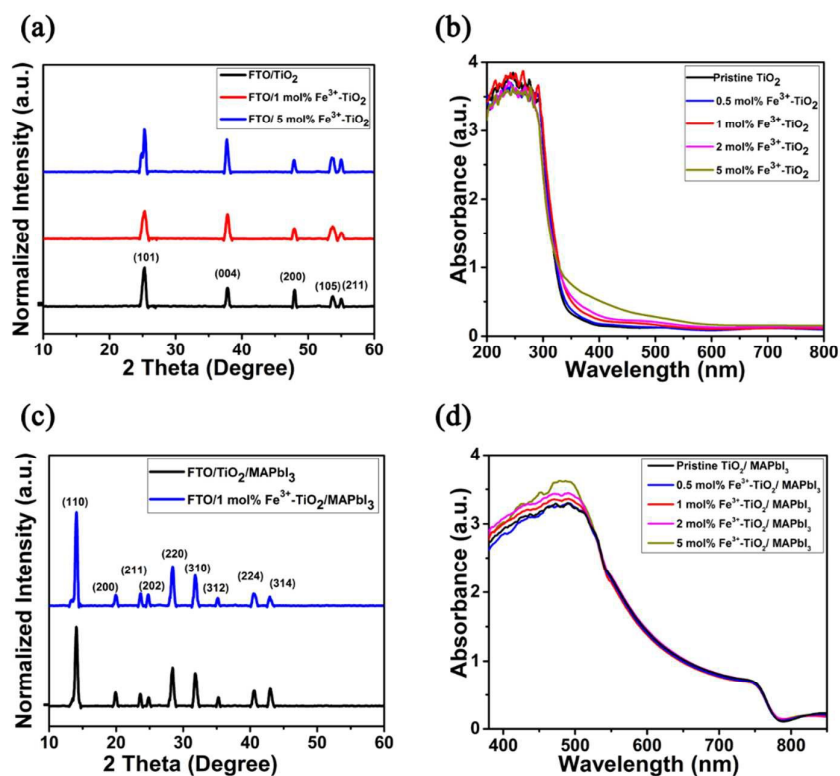


**Fig. 2** (a) XRD pattern of pristine TiO<sub>2</sub> and Fe<sup>3+</sup>-TiO<sub>2</sub>. (b) The UV-vis absorption curves of the pristine TiO<sub>2</sub> or Fe<sup>3+</sup>-TiO<sub>2</sub> compact layer. (c) XRD patterns of MAPbI<sub>3</sub> thin films with doped and pure TiO<sub>2</sub> compact layer. (d) Absorption lines of the cells with the following structure: FTO/ TiO<sub>2</sub> or Fe<sup>3+</sup>-TiO<sub>2</sub>/ MAPbI<sub>3</sub>.

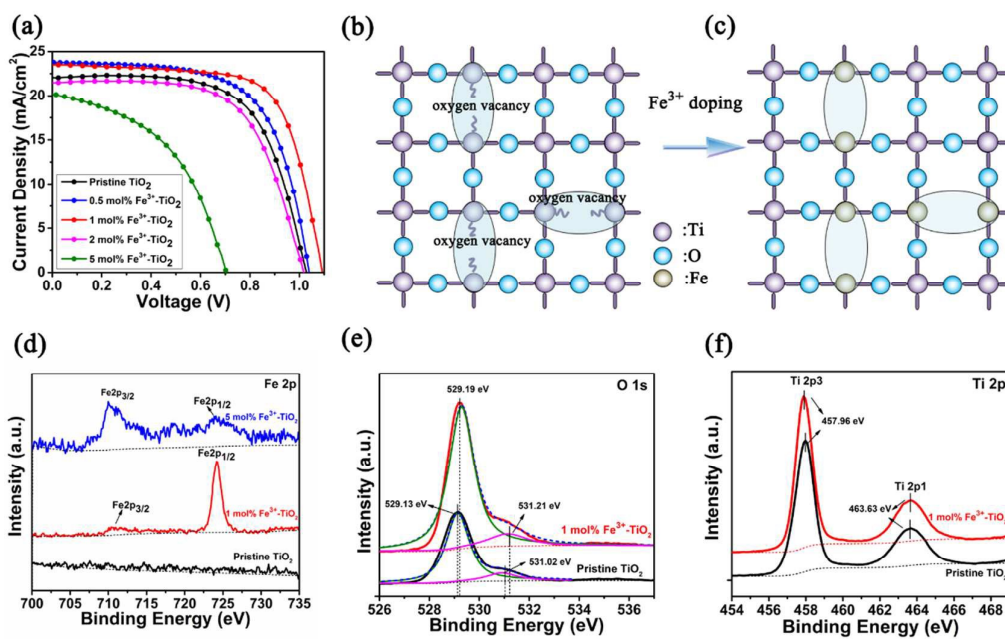


**Fig. 3** (a) J-V curves of the TiO<sub>2</sub>-based and Fe<sup>3+</sup>-TiO<sub>2</sub>-based MAPbI<sub>3</sub> solar cells. (b) Defects in the pristine TiO<sub>2</sub>. (c) Fe<sup>3+</sup> substitution at the Ti<sup>3+</sup> sites passivates oxygen vacancy defects. (d) XPS spectra of pristine TiO<sub>2</sub> and Fe<sup>3+</sup>-TiO<sub>2</sub>. (e) XPS spectra of O 1s peaks for pristine TiO<sub>2</sub> and 1 mol% Fe<sup>3+</sup>-TiO<sub>2</sub> samples. (f) XPS spectra of Ti 2p peaks.

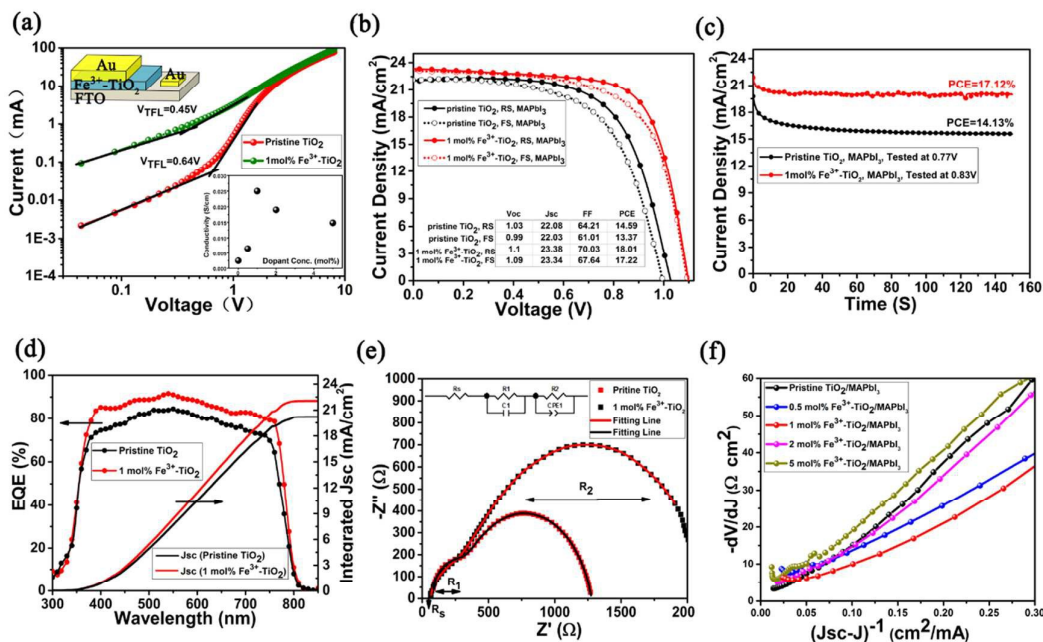


**Fig. 4** (a) Log-log plot of I-V curves of Fe<sup>3+</sup>-TiO<sub>2</sub> and TiO<sub>2</sub> devices with the structure of FTO/ Fe<sup>3+</sup>-TiO<sub>2</sub> (or TiO<sub>2</sub>) /Au. (b) J-V curves of the FTO/ 1 mol% Fe<sup>3+</sup>-TiO<sub>2</sub> (or TiO<sub>2</sub>)/ meso-TiO<sub>2</sub>/ MAPbI<sub>3</sub>/ Spiro-OMeTAD/ Au cells. (c) Steady-state current density of the Fe<sup>3+</sup>-TiO<sub>2</sub>-based and TiO<sub>2</sub>-based cells. (d) EQE curves and integrated current density of Fe<sup>3+</sup>-TiO<sub>2</sub>-based and TiO<sub>2</sub>-based MAPbI<sub>3</sub> cells. (e) Nyquist plot of the MAPbI<sub>3</sub>-based cells with the following structure: FTO/ TiO<sub>2</sub> or Fe<sup>3+</sup>-TiO<sub>2</sub>/ meso-TiO<sub>2</sub>/ MAPbI<sub>3</sub>/ Spiro-OMeTAD/ Au. (f) -dV/dJ vs. (J<sub>sc</sub>-J)<sup>-1</sup> curves in the approximately linear region of the PSCs.

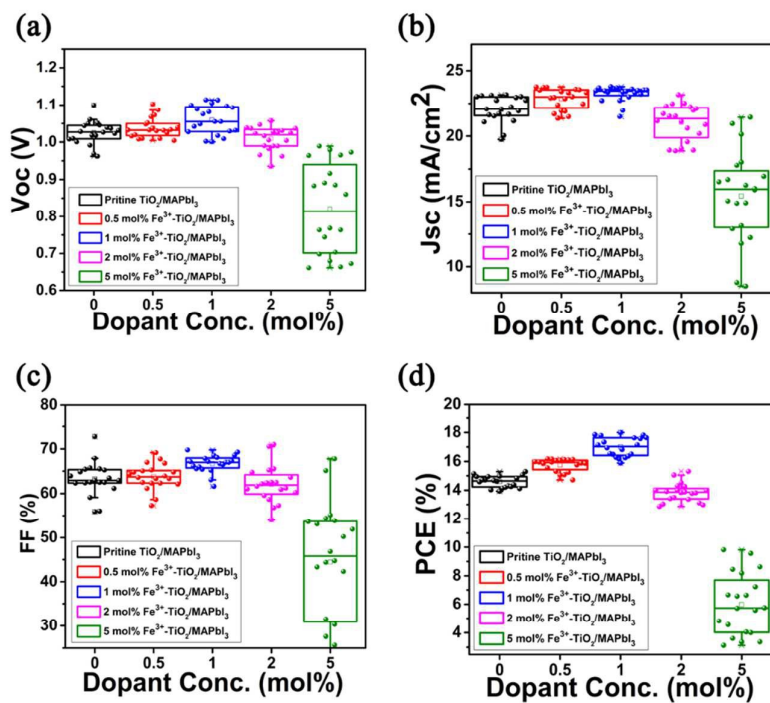


**Fig. 5** The photovoltaic parameters' statistical distribution of the MAPbI<sub>3</sub>-based PSCs with different Fe<sup>3+</sup>-doping concentrations. (a) Distribution of Voc. (b) Distribution of Jsc. (c) Distribution of FF. (d) Distribution of PCE.

**Table 1** The ratios of Fe/Ti in 5 mol% Fe<sup>3+</sup>-doped compact TiO<sub>2</sub> film measured by EDS analysis.

| position | Fe/Ti (%) |
|----------|-----------|
| 1        | 5.9       |
| 2        | 5.7       |
| 3        | 6.5       |
| 4        | 7.1       |
| 5        | 6.8       |
| Average  | 6.4       |

**Table 2** The theoretical and experimental atomic ratios of Fe/Ti for pristine and Fe<sup>3+</sup>-doped TiO<sub>2</sub>.

| Sample                                    | Fe/Ti (%)         |              |
|---|-------------------|--------------|
|   | Theoretical value | XPS analysis |
| Pristine TiO <sub>2</sub>                 | 0                 | 0            |
| 1 mol%-Fe <sup>3+</sup> -TiO <sub>2</sub> | 1                 | 1.37         |
| 5 mol%-Fe <sup>3+</sup> -TiO <sub>2</sub> | 5                 | 6.41         |

**Table 3** The parameters (mean value based on 100 Cells) of MAPbI<sub>3</sub> solar cells with different Fe<sup>3+</sup>-doping concentrations in TiO<sub>2</sub> compact layer.

| Sample                                      | Voc (V) | Jsc (mA/cm <sup>2</sup> ) | FF (%) | N    | PCE (%) |
|---|---------|---------------------------|--------|------|---------|
| Pristine TiO <sub>2</sub>                   | 1.02    | 22.03                     | 63.25  | 3.99 | 14.59   |
| 0.5 mol% Fe <sup>3+</sup> -TiO <sub>2</sub> | 1.04    | 22.84                     | 63.77  | 3.38 | 15.74   |
| 1 mol% Fe <sup>3+</sup> -TiO <sub>2</sub>   | 1.06    | 23.22                     | 66.68  | 2.95 | 17.01   |
| 2 mol% Fe <sup>3+</sup> -TiO <sub>2</sub>   | 1.01    | 21.03                     | 62.07  | 4.58 | 13.85   |
| 5 mol% Fe <sup>3+</sup> -TiO <sub>2</sub>   | 0.82    | 15.44                     | 44.45  | 8.04 | 5.98    |



**For Table of Contents Entry**

The PCE of perovskite solar cell based on  $\text{Fe}^{3+}$ -doped compact  $\text{TiO}_2$  is improved from 16.02% to 18.60%.

